

RSC Advances



This is an *Accepted Manuscript*, which has been through the Royal Society of Chemistry peer review process and has been accepted for publication.

Accepted Manuscripts are published online shortly after acceptance, before technical editing, formatting and proof reading. Using this free service, authors can make their results available to the community, in citable form, before we publish the edited article. This *Accepted Manuscript* will be replaced by the edited, formatted and paginated article as soon as this is available.

You can find more information about *Accepted Manuscripts* in the [Information for Authors](#).

Please note that technical editing may introduce minor changes to the text and/or graphics, which may alter content. The journal's standard [Terms & Conditions](#) and the [Ethical guidelines](#) still apply. In no event shall the Royal Society of Chemistry be held responsible for any errors or omissions in this *Accepted Manuscript* or any consequences arising from the use of any information it contains.

COMMUNICATION

Polymer nanocomposites from free-standing, macroscopic boron nitride nanotube assemblies

Cite this: DOI: 10.1039/x0xx00000x

Keun Su Kim,^a Michael B. Jakubinek,^a Yadienka Martinez-Rubi,^a Behnam Ashrafi,^b Jingwen Guan,^a K. O'Neill,^b Mark Plunkett,^a Amy Hrdina,^a Shuqiong Lin,^a Stéphane Dénomée,^a Christopher Kingston^a and Benoit Simard^{*a}

Received 00th January 2012,
Accepted 00th January 2012

DOI: 10.1039/x0xx00000x

www.rsc.org/

Here we report fabrication of free-standing boron nitride nanotube (BNNT) sheets by direct deposition and by vacuum filtration methods, including novel hybrid assemblies with BNNT and carbon nanotubes. Such sheets have enabled production of polymer nanocomposites with high nanotube content. Two example cases, BNNT-epoxy nanocomposites (>30 wt.% BNNTs) produced by impregnation of dry sheets and BNNT sheets modified by integration of a thermoplastic polyurethane are described. Related methods have proven advantageous for carbon nanotube composites and, enabled by new technology for large scale BNNT production, such composites have now been realized with BNNTs. This represents an important milestone towards the development of BNNT-based multifunctional composites.

Boron nitride nanotubes (BNNTs) exhibit a range of properties that are as impressive as those of carbon nanotubes (CNTs),¹⁻⁵ including comparable mechanical properties and thermal conductivity,^{6,7} but with substantially higher thermal stability (greater than 800 °C in air) and,⁸ unlike CNTs, polarizability,⁹ wide band gap of ~5 eV,¹⁰ transparency in the visible region, and ability to shield neutron radiation.⁵ These unique characteristics make BNNTs attractive in the development of high-performance, light-weight polymer nanocomposites, with potential to impact a range of engineering sectors such as aerospace and armour materials.¹¹⁻¹⁸

To fully realize this potential it is important to develop diverse BNNT-polymer nanocomposite systems and architectures, including those with high fractions of BNNTs.¹⁷ For example, it was demonstrated that effective improvement in thermal conductivity was achieved at high loadings of over 10 wt. %.¹⁸ Further, as demonstrated

in the CNT literature, one of the most effective ways to produce CNT-enhanced polymer nanocomposites is through resin-infiltration of macroscopic assemblies of nanotubes such as yarns, thin films or sheets.¹⁹⁻²¹ This technique has advantages over dispersion/mixing approaches in terms of scalability, materials handling, consistency of the nanotube distribution in the composite and especially for achieving high nanotube content. Composites with a high fraction of CNTs (up to 40 wt.%) have been reported by this approach.¹⁹ However, there have been very few attempts to fabricate BNNT nanocomposites using this technique, mainly due to the low accessibility of large quantities of BNNTs and the resulting lack of development of methods for making free-standing macroscopic assemblies of BNNTs. The only example of this approach was demonstrated by soaking a BNNT mat supported on a filter membrane in a polymer solution for a week and achieved a high BNNT loading of 18-37 wt.%.²²

The National Research Council Canada (NRC) has recently addressed the BNNT supply limitation through the development of a patent-pending, industrially scalable plasma process for BNNT production.^{23,24} Other approaches including a laser-based method²⁵ and a second plasma method²⁶ also have been developed recently. With these advances in the supply of high-quality BNNTs, development of BNNT composites is positioned to advance quickly. The NRC method, called hydrogen-assisted BNNT synthesis (HABS), makes use of hydrogen, which dramatically increases yield relative to most earlier high-temperature processes, to produce BNNTs without metal catalyst.²⁴ The method produces few-walled, highly crystalline small-diameter BNNTs (~5 nm diameter) at rates now approaching 30 g/h, which effectively removes previous supply limitations to the development of BNNT composites. It is also observed that the diversity in the macroscopic morphology of the as-produced BNNT materials from the HABS process (see Fig. 1) lends to its easy adaption in

fabricating macroscopic BNNT assemblies,²⁴ which are highly advantageous in the manufacturing of BNNT composites with high fraction of nanotubes. Here we report the fabrication of BNNT-polymer nanocomposites, including BNNT-epoxy and BNNT-polyurethane, for the first time from free-standing, nanotube papers (often called *buckypaper* in the carbon nanotube literature), demonstrating that this approach and its advantages are now accessible and effective for production of high nanotube content BNNT composites. In addition, new macroscopic BNNT assemblies (anisotropic BNNT sheets and CNT/BNNT heterobuckypapers) are reported and present new possibilities for multifunctional nanocomposites.

In this work, BNNTs were synthesized from hBN via the HABS process, post-purified, and then formed into BNNT buckypapers by solvent dispersion and vacuum filtration similar to typical procedures employed in production of CNT buckypaper. (Additional details on the BNNTs and buckypaper production methods are provided as Supplementary Information, including Figs. S1 to S4.) The free-standing BNNT buckypapers (Fig. 2a) produced from purified BNNT dispersions provided good structural integrity. The filtration method was directly scaled up to 30 cm × 30 cm and subsequently adapted to produce 30 cm × 1 m sheets (see, also, Fig. S4). The typical physical and mechanical properties of pristine BNNT buckypapers are summarized in Table 1. The fabricated BNNT buckypapers are flexible and foldable, and leverage the multifunctional properties of BNNTs. For example, the inset of Fig. 2a shows a BNNT paper airplane in a natural gas flame, illustrating its foldability and high flame resistance. BNNT buckypaper is stable without any structural deformation over extended periods in the flame due to the high thermal stability of BNNTs (see Fig. S5 for comparison to CNT and cellulose-based papers). The thermal stability was also assessed by TGA, showing stability in air to over 900 °C (see Fig. S3). Hence, BNNTs offer an obvious advantage over CNTs for flame and high-temperature resistant nanocomposite applications.

We also demonstrated the fabrication of heterostructured buckypapers using similar dispersion-filtration techniques, which offer the potential for additional sets of multifunctional properties due to the discrete properties of the individual layers. Figures 2b and 2e show two heterobuckypapers composed of both CNTs and BNNTs. The first heterobuckypaper shown in Fig. 2b has CNT and BNNT layers on opposite sides, and is coined a “Janus buckypaper” after the two-faced Roman god *Janus* and similar to the convention used for comparable heterostructured particles.²⁷ The second heterobuckypaper shown in Fig. 2e is a sandwich cookie structure consisting of alternating layers of CNT, BNNT and CNT. The optical microscope image in Fig. 2g shows that these are well-defined layers approximately 50 μm in thickness. These novel structures can offer additional functionalities over homogeneous buckypapers and may be of particular interest for polymer composite applications. For instance, structures with highly anisotropic electrical properties (e.g., for insulated high-temperature wire, see Fig. S6), or to combine electromagnetic and neutron shielding capabilities. The highly-conductive CNTs and high relative permittivity and dielectric strength of BNNTs present the opportunity to produce entirely nanotube-based capacitors.²⁸ We demonstrate flexible all-nanotube capacitors in Fig. 2h and Fig. S7. Using an LCR meter to measure capacitance and treating the structure as a parallel plate capacitor indicates an apparent dielectric constant of $\kappa \sim 3$ and 0 μA

leakage for the sandwich cookie buckypaper heterostructure. Applications and detailed physico-chemical properties of such heterobuckypapers are currently under investigation.

BNNT buckypaper structures can also be produced in situ within the synthesis reactor. Figure 3 shows a BNNT sheet (12.7 cm × 11.3 cm) formed on a rotating cylinder that was placed within the reactor during a BNNT synthesis run (see also Fig. S8), inspired by previous demonstrations for CNTs.^{29,30} This as-produced BNNT sheet (Fig. 3b) is flexible and mechanically robust. Its mechanical properties are summarized in Fig. 3c. The lower strength and stiffness compared to the BNNT buckypapers prepared by post-processing can be understood due to its lower density (0.16 g/cm³). Interestingly, this BNNT sheet exhibits anisotropy in strength and stiffness, unlike the buckypapers formed from the post-processing method. Higher strength and stiffness are obtained along the direction of rotation of the cylinder (i.e., length direction). This observation is attributed to partial alignment of the BNNTs along the rotation direction (see Fig. 3d).

The BNNT sheet assemblies described above provide a platform for high-nanotube content composites previously reported for CNTs. Such nanocomposites were demonstrated by using pristine BNNT buckypapers prepared by post-processing. The first example is an epoxy-infiltrated BNNT buckypaper composite (Fig. 4) made by infusing a low viscosity, aerospace-grade epoxy resin (Araldite MY0510 with Aradur HT 976, 4,4'-diaminodiphenylsulfone curing agent) into a BNNT buckypaper. Impregnation of small pieces of BNNT buckypaper (3.5 cm × 5.0 cm; ~60 μm thick) was implemented through pure capillary force. Prior to the impregnation step, a hot-plate was used to heat the buckypaper to approximately 100°C. The epoxy resin, pre-heated to 100°C, was poured on top of the BNNT buckypaper and, after infiltration, excess resin was wiped off using lint-free absorbent wipes. The sample was then placed between glass plates with a small weight to avoid any warpage of the sample and oven-cured according the manufacturer recommended curing protocol (120°C for 2 h with postcuring at 177°C for 2 h).

Figure 4a shows a photo of epoxy-impregnated BNNT buckypaper composite with 32 wt.% nanotube content. Unlike polymer-impregnated CNT buckypapers, this BNNT-epoxy composite is semi-transparent. The BNNT content was determined from the areal density (g/cm²) before and after resin impregnation and verified by TGA (e.g., Fig. 4b). Given the temperature stability of BNNTs and that the residue from combustion of the epoxy was negligible, TGA provides a more ideal tool for quantifying composition in this case than it does for CNT buckypapers. TGA is effective even for BNNT buckypapers with a significant boron impurity, in which case masses can be taken before the mass curve increases due to boron oxidation (see Fig. S3). Figure 4c is a SEM image of a resin-infiltrated BNNT composite taken from the cross-sectional area of a fractured specimen. This image shows significant pull-out of BNNT ropes, which is an effective energy absorbing mechanism during failure of fiber-reinforced composites. This phenomenon also can be seen in CNT buckypaper composites.²¹ A good interaction (i.e., wetting of BNNT with resin) can be observed in this SEM image as well as in a contact angle image in Fig. 4a. The initial contact angles were below 60° indicating wetting of the surface.

Table 1 summarizes the measured physical and mechanical properties of BNNT buckypaper before and after resin impregnation. After impregnation, the void content decreased from 80% to less than

5%, suggesting that nearly full impregnation of the BNNT buckypaper was achieved. For pristine BNNT buckypaper, the Young's modulus was ~ 0.5 GPa and the ultimate tensile strength was ~ 2 MPa. After epoxy-impregnation, the Young's modulus is improved by almost 20 fold (to 7.7 GPa) as compared to the pristine BNNT buckypaper (0.37 GPa) and a factor of 2 higher than the neat epoxy. Dynamic mechanical analysis (DMA) measurements also verify increased stiffness ($> 2\times$ higher storage modulus than the neat epoxy near room temperature), but with several degrees decrease in glass transition temperature observed from the shift in the $\tan(\delta)$ peak (Fig. S9). The ultimate tensile strength of the composite (42 MPa) shows a 20 fold enhancement versus the pristine BNNT buckypaper. However, this value is still only about 60 % that of the neat epoxy (~ 71 MPa). Measured strain at failure of 0.6% indicates the brittleness of the composite. Improvements in BNNT purity and the impregnation method, as well as stronger interaction between BNNTs and epoxy (e.g., by using functionalization such as employed for CNT buckypapers)^{31,32} should further improve the mechanical properties and are the subject of current studies.

In a second example, polymer nanocomposites were prepared by using thermoplastic polyurethane (TPU; UAF 472 by Adhesive Films Inc.) to modify the buckypaper properties. The TPU-modified BNNT buckypaper composites (Fig. 5) were prepared by both (1) infiltration of preformed buckypapers and (2) a one-step filtration method using a BNNT/TPU suspension. In the infiltration method the pristine buckypaper was immersed in a TPU solution in THF (40 mg/mL) for 24 h before removing the solution and drying on a Teflon film, resulting in a BNNT:TPU ratio of 83:17 by weight. In the one-step filtration method TPU and purified BNNTs were mixed at a 5:1 weight ratio in tetrahydrofuran (THF) or THF/methanol mixtures. After bath sonication for 30 min to form a homogeneous suspension, the suspension was filtered through a PTFE filter membrane (0.2 μm pore diameter) and the composite was sandwiched between sheets of parchment paper and dried at room temperature overnight.

Table 2 summarizes BNNT/TPU samples prepared for this study. After the infiltration (i.e., simply soaking the nanotube buckypaper in a TPU solution for 24 h), the buckypaper density increased from 0.38 g/cm^3 to 0.50 g/cm^3 . Note that unlike the nanocomposites formed by epoxy-impregnation, these sheets retain the porous character of buckypaper. It was found that increasing the concentration of the TPU solution or the infiltration time did not increase significantly the TPU content in the nanocomposite during the infiltration. As demonstrated in Fig. 5a and 5b, the nanocomposites are flexible, mechanically robust and semi-transparent. A summary of mechanical properties is shown in Figs. 5d and 5e. The pristine BNNT buckypaper in this case presented a Young's modulus of 0.245 GPa, an ultimate tensile strength of ~ 1 MPa and a strain at failure of 0.4 % while the neat TPU resin presents a Young's modulus of 0.056 GPa, a yield strength of 5 MPa. After incorporation of the TPU in the preformed BNNT buckypaper, the elastic modulus and the failure strength showed 2 and 5 fold improvements, respectively, while the elongation at break improved by 4.5 fold compared to the pristine BNNT buckypaper.

In the one-step filtration method, the use of a combination of different volume ratios of good and bad solvents for TPU (i.e., THF and methanol) proved to be effective in controlling the BNNT/TPU ratio in the final nanocomposite; as the content of the bad solvent (methanol) was increased in the solvent mixture, the TPU content in a composite

increased. The density also increased with the TPU content but a significant void content is still present in all samples. FTIR spectra recorded in attenuated total reflectance (ATR) configuration show signals for TPU and BNNTs even in cases where TPU is present at < 10 wt.% (see Fig S10). For the samples with high BNNT:TPU ratio and low density, the best mechanical properties were observed for the case of BN75PU25 (i.e., 75% BNNTs and 25% TPU by weight), which showed improvements in elastic modulus, ultimate tensile strength and strain at failure of 4.4 fold, 8 fold, and 7 fold, respectively, compared to pristine BNNT buckypaper. While at low TPU-content the polymer improves the buckypaper properties, at high TPU-content the properties are qualitatively different and more resemble the TPU polymer. In the latter case, the nanocomposites are lower stiffness, higher density, and have much higher strain at failure (~ 2000 times higher than the BNNT buckypaper) approaching that of neat TPU. Accordingly, the one-step filtration method appears to be effective for the fabrication of light-weight (0.5 g/cm^3), high BNNT content nanocomposites with improved and tailor-able mechanical properties. Due to its porous character, TPU-modified BNNT buckypapers also can serve as an intermediate to preparation of other high-BNNT content polymer nanocomposites.

Conclusions

The accessibility of commercial-scale quantities of BNNTs and their macroscopic assemblies has been a significant challenge in the realization of various BNNT-based multifunctional materials, especially in nanocomposite applications with high fractions of BNNTs.¹⁸ By leveraging a recent advancement in BNNT production technology,²⁴ we have demonstrated the production of BNNT-polymer nanocomposites with high BNNT content, for the first time by resin-infiltration of free-standing BNNT buckypaper assemblies with both epoxy and TPU resins. The epoxy composite showed large improvements in both modulus and ultimate tensile strength compared to a pristine BNNT buckypaper, and a 2 fold improvement in modulus when compared to the bulk resin. The TPU-modified BNNT buckypaper nanocomposites showed promising improvements, including significant increases in yield strength, modulus and strain at failure compared to unmodified BNNT buckypaper and tailorable properties that become more TPU-like, with high strain at failure, as the BNNT:TPU weight ratio decreases. Realization of BNNT buckypaper-based nanocomposites with high nanotube content, which have proven advantageous in the carbon nanotube field, is an important step in the development of BNNT composites for structural and multifunctional applications. As such, it would also be interesting to examine other properties such as thermal or electrical properties. Novel heterostructures produced with CNT and BNNT layers were also demonstrated and represent opportunities for new, multifunctional composites that leverage the anisotropic properties across the different layers, including for insulated conductors, flame resistance, capacitors and other cases.^{33,34}

Notes and references

^a Security and Disruptive Technologies Portfolio, National Research Council Canada, 100 Sussex Dr., Ottawa, Canada. Fax: 1-613-991-2648; Tel: 1-613-990-0977; Benoit.Simard@nrc-cnrc.gc.ca

^b *Aerospace Portfolio, National Research Council Canada, 5145 Decelles Av., Montreal, Canada.*

† Electronic Supplementary Information (ESI) available: Additional description of the experimental methods and characterization, as well as supplementary figures referenced in the main text. See DOI: 10.1039/c000000x/

- 1 N. G. Chopra, R. J. Luyken, K. Cherrey, V. H. Crespi, M. L. Cohen, S. G. Louie and A. Zettl, *Science*, 1995, **269**, 966-967.
- 2 D. Golberg, Y. Bando, C. C. Tang and C. Y. Zhi, *Adv. Mater.*, 2007, **19**, 2413-2432.
- 3 C. N. R. Rao and A. Govindaraj, *Adv. Mater.*, 2009, **21**, 4208-4233.
- 4 R. Arenal, X. Blase and A. Loiseau, *Adv. Phys.*, 2010, **59**, 101-179.
- 5 M. L. Cohen and A. Zettl, *Phys. Today*, 2010, **63**, 34-38.
- 6 D. Golberg, Y. Bando, Y. Huang, T. Terao, M. Mitome, C. Tang and C. Zhi, *ACS Nano*, 2010, **4**, 2979-2993.
- 7 C. Zhi, Y. Bando, C. C. Tang and D. Golberg, *Mater. Sci. Eng. R*, 2010, **70**, 92-111.
- 8 Y. Chen, J. Zou, S. J. Campbell and G. Le Caer, *Appl. Phys. Lett.*, 2004, **84**, 2430-2432.
- 9 S. M. Nakhmanson, A. Calzolari, V. Meunier, J. Bernholc and M. Buongiorno-Nardelli, *Phys. Rev. B*, 2003, **67**, 235406.
- 10 A. Rubio, J. L. Corkill and M. L. Cohen, *Phys. Rev. B*, 1994, **49**, 5081-5084.
- 11 C. Y. Zhi, Y. Bando, C. C. Tang, Q. Huang and D. Golberg, *J. Mater. Chem.*, 2008, **18**, 3900-3908.
- 12 C. Y. Zhi, Y. Bando, C. Tang, H. Kuwahara and D. Golberg, *J. Nanomater.*, 2008, 642036.
- 13 C. Y. Zhi, Y. Bando, T. Terao, C. C. Tang, H. Kuwahara, D. Golberg, *Chem. Asian J.*, 2009, **4**, 1536-1540.
- 14 K. Nogi, M. Hosokawa, M. Naito and T. Yokoyama (eds), *Nanoparticle Technology Handbook*, Elsevier, 2012, Application 50, 629-367.
- 15 X. Huang, C. Zhi, P. Jiang, D. Golberg, Y. Bando and T. Tanaka, *Adv. Funct. Mater.*, 2013, **23**, 1824-1831.
- 16 H. Yan, Y. Tang, J. Su and X. Yang, *Appl. Phys. A*, 2014, **114**, 331-337.
- 17 A. L. Tian *et al.*, *Biosensors, and Info-Tech Sensors and Systems 2014*, V. K. Varadan (eds), *Proc. of SPIE*, 2014, **9060**, 906006.
- 18 W. Meng, Y. Huang, Y. Fu, Z. Wang and C. Zhi, *J. Mater. Chem. C*, 2014, **2**, 10049-10061.
- 19 Z. Wang, Z. Liang, B. Wang, C. Zhang and L. Kramer, *Compos. Part A*, 2004, **35** 1225-1232.
- 20 S. Wang, Z. Liang, G. Pham, Y.-B. Park, B. Wang, C. Zhang, L. Kramer and P. Funchess, *Nanotechnology* 2007, **18**, 095708.
- 21 B. Ashrafi, J. Guan, V. Mirjalili, P. Hubert, B. Simard and A. Johnston, *Compos. Part A*, 2010, **41**, 1184-1191.
- 22 C. Y. Zhi, Y. Bando, T. Terao, C. Tang, H. Kuwahara and D. Golberg, *Adv. Funct. Mater.*, 2009, **19**, 1857-1862.
- 23 K. S. Kim, C. Kingston and B. Simard. Patent App. No. US61/813,324, 2013.
- 24 K. S. Kim, C. T. Kingston, A. Hrdina, M. B. Jakubinek, J. Guan, M. Plunkett and B. Simard, *ACS Nano* 2014, **8**, 6211-6220.
- 25 M. W. Smith, K. C. Jordan, C. Park, J.-W. Kim, P. T. Lillehei, R. Crooks and J. S. Harrison, *Nanotechnology*, 2009, **20**, 505604.
- 26 A. Fathalizadeh, T. Pham, W. Mickelson and A. Zettl, *Nano Lett.*, 2014, **14**, 4881-4886.
- 27 S. Granick, S. Jiang and Q. Chen, *Phys. Today*, 2009, **62**, 68-69
- 28 D. Santiago, J. Hurst, J. Wu, M. Lebron-Colón. Hybrid BNNT-C nanostructure supercapacitor with high energy density. http://nari.arc.nasa.gov/sites/default/files/10_Santiago_ARMD_PhaseI_NARI.pdf (Mar. 2012; last accessed Jan. 19, 2015).
- 29 Y. -L. Li, I. A. Kinloch and A. H. Windle, *Science*, 2004, **307**, 276-278.
- 30 X. -H. Zhong, Y. -L. Li, J. -M. Feng, Y. -R. Kang and S. -S. Han, *Nanoscale*, 2012, **4**, 5614-5618.
- 31 Y. Martinez-Rubi, B. Ashrafi, J. Guan, C. Kingston, A. Johnston, B. Simard, V. Mirjalili, P. Hubert, L. Deng and R. J. Young, *ACS Appl. Mater. Interfaces*, 2011, **3**, 2309-2317.
- 32 M. B. Jakubinek, B. Ashrafi, J. Guan, M. B. Johnson, M. A. White, B. Simard. *RSC Advances*, 2014, **4**, 57564-57573
- 33 T. Terao, C. Zhi, Y. Bando, M. Mitome, C. Tang and D. Golberg, *J. Phys. Chem. C*, 2010, **114**, 4340-4344.
- 34 C. W. Chang, A. M. Fennimore, A. Afanasiev, D. Okawa, T. Ikuno, H. Garcia, Deyu Li, A. Majumdar and A. Zettl, *Phys. Rev. Lett.*, 2006, **97**, 085901.

Table 1. Physical and mechanical properties of pristine and epoxy-infiltrated BNNT buckypaper sheets.

Sample	Density (g/cm ³)	Void Content (%)	Young's Modulus (GPa)	Ultimate Tensile Strength (MPa)	Strain at Failure (%)
Pristine BNNT BP	0.43	80%	0.37	2	0.8
BNNT BP/epoxy	1.34	5%	7.7	42	0.6

Note: According to the epoxy resin manufacturer, Young's modulus, ultimate tensile strength and strain failure of 3.5 GPa, 71 MPa and 2.7%, respectively, are reported for the bulk resin.

Table 2. Physical properties of pristine and BNNT-polyurethane nanocomposites

Sample	Method	Solvent	BNNT:TPU (wt. ratio)	Density (g/cm ³)	Void Content
BNNT	Filtration	Methanol	NA	0.38	80
BN83PU17	Infiltration	THF	83:17	0.50	72
BN93PU7	On-step filtration	THF	93:7	0.51	72
BN75PU25	On-step filtration	THF/Methanol (1:0.8)	75:25	0.59	66
BN25PU75	On-step filtration	THF/Methanol (1:1)	25:75	0.75	45

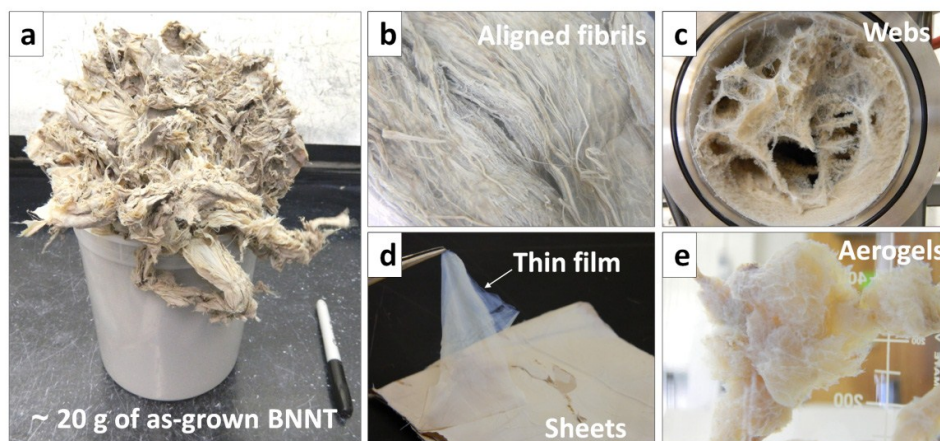


Figure 1. Photographs of as-produced BNNT materials with different macroscopic morphologies. (a) Reaction product in bulk (~20 g). (b) Fibril-like BNNT materials. (c) Aerogel and web-like materials. (d) Sheets and thin films. (e) Aerogel-like materials.

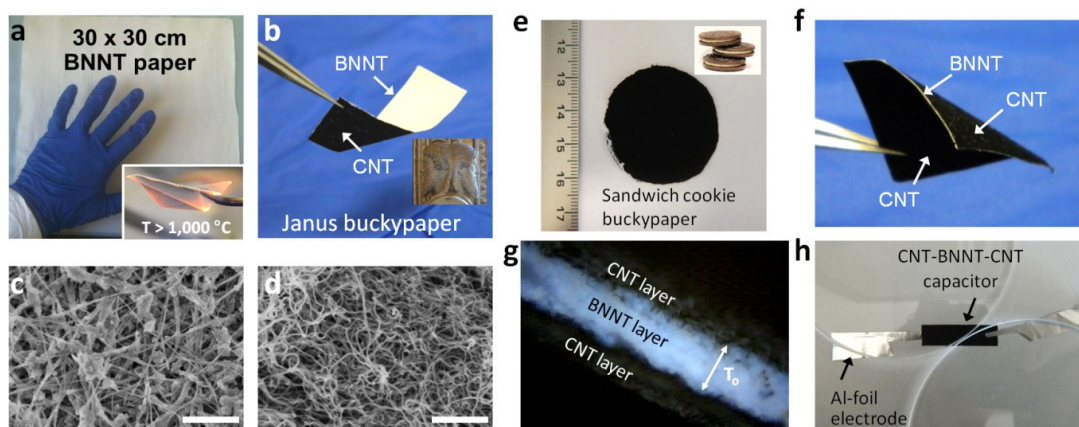


Figure 2. BNNT and heterostructured buckypapers. (a) Photograph of pristine BNNT buckypaper. Inset is a flame test of a BNNT paper airplane (see Fig. S4 for additional information). (b) Photograph of *Janus* buckypaper composed of two different surfaces of BNNT and CNT. (c), (d) SEM images of *Janus* buckypaper showing (c) the BNNT and (d) the CNT surfaces, respectively. The scale bars are 0.5 μm . (e), (f) Photographs of sandwich cookie buckypaper composed of three consecutive layers of CNT/BNNT/CNT. (g) Optical image showing the cross section of sandwich cookie buckypaper. The thickness (T_0) of the BNNT layer is $\sim 50 \mu\text{m}$. (h) A flexible capacitor implemented with sandwich cookie buckypaper.

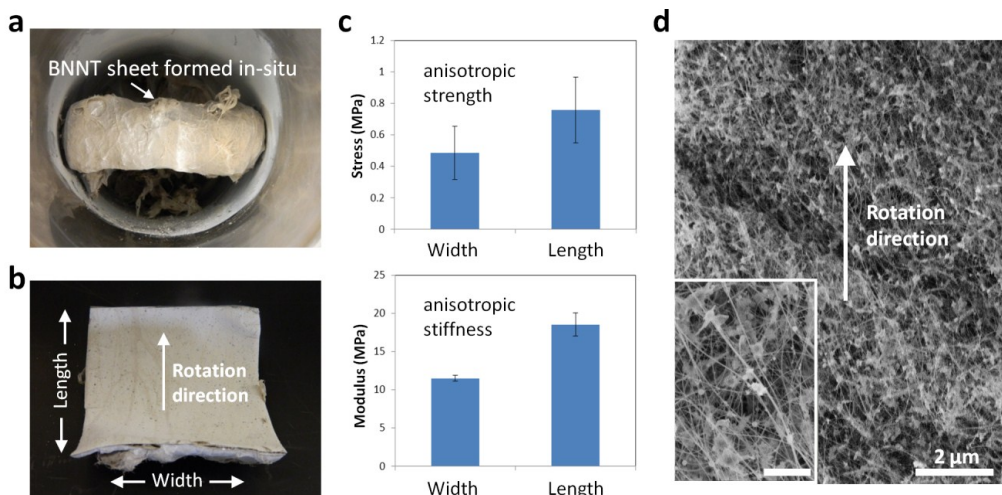


Figure 3. (a), (b) As-produced BNNT sheet ($12.7 \text{ cm} \times 11.3 \text{ cm}$; 0.16 g/cm^3) formed in-situ during the BNNT synthesis. (c) Results of mechanical properties of the BNNT sheet in two different directions (length and width directions). (d) SEM images of the BNNT sheet showing partial preferential alignment of BNNT along the rotation direction. The scale bar in the inset is 500 nm.

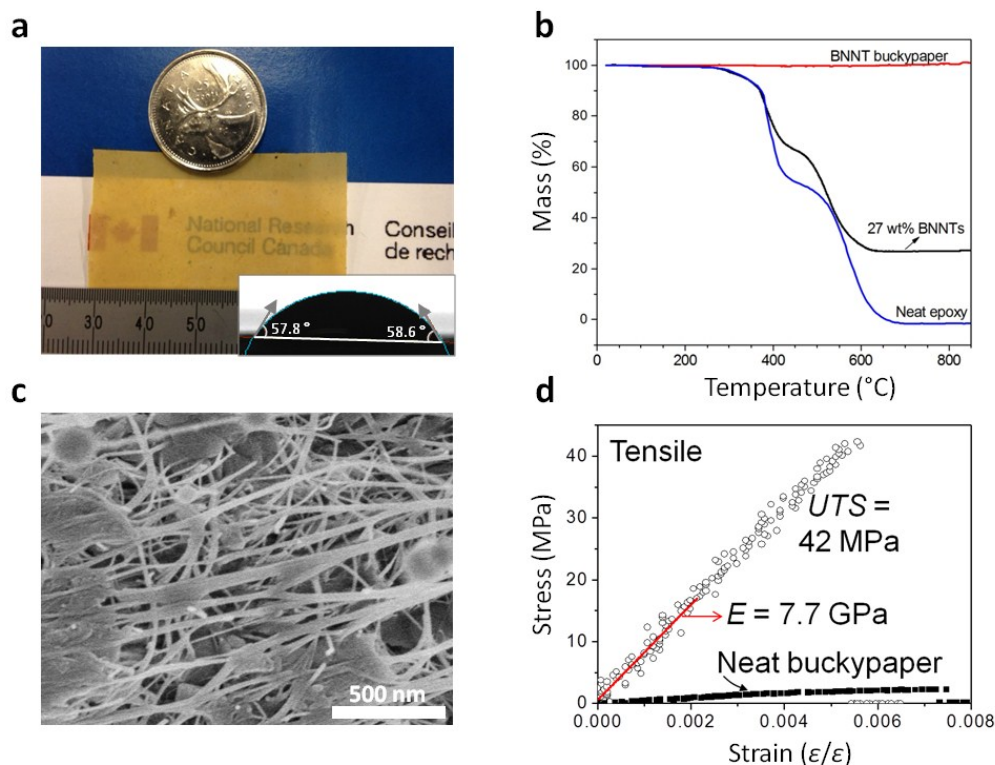


Figure 4. BNNT-epoxy composite. (a) Photograph of a $60 \mu\text{m}$ thick BNNT buckypaper infiltrated by an epoxy resin (32 wt. % of BNNT). Inset is a contact angle measurement of the epoxy resin on a pristine BNNT buckypaper. The initial contact angles were below 60° indicating wetting of the surface. (b) TGA in oxidation mode verifying BNNT content in the buckypaper composites (c) SEM image of the cross-sectional area of a resin-infiltrated BNNT buckypaper. (d) Tensile properties of pristine and epoxy-infiltrated BNNT buckypaper sheets.

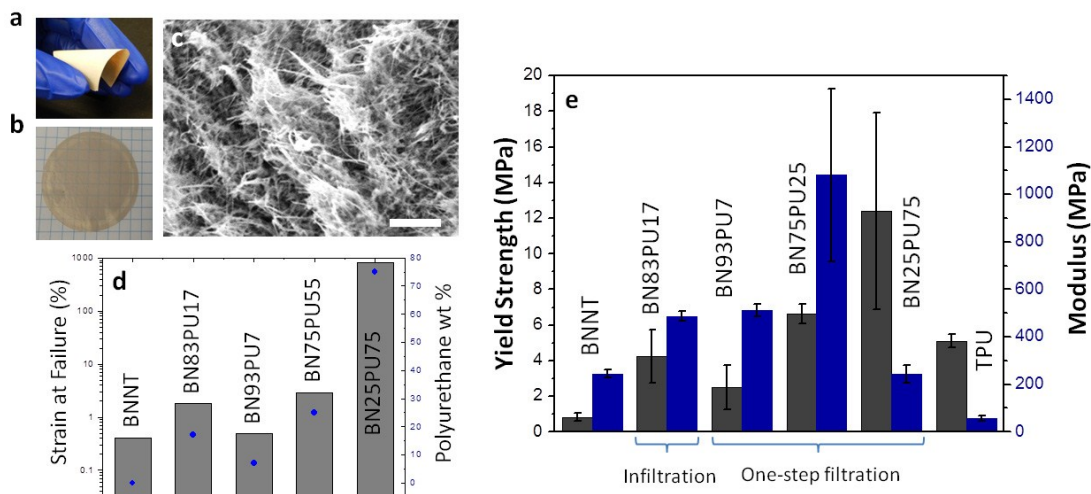


Figure 5. TPU-modified BNNT buckypaper composites. (a) Photograph of 75 μm and (b) 35 μm thick composites obtained by the infiltration and one-step filtration methods, respectively. (c) SEM image of the cross-sectional area of a resin-infiltrated BNNT buckypaper (BN83PU17). The scale bar is 1 μm . (d), (e) Tensile properties of the neat TPU, pristine BNNT buckypaper and nanocomposite samples.